Modeling and simulation of a compressor installed with active magnetic bearings exploiting feedforward control

Modeling and Simulation of a Compressor Installed with Active Magnetic Bearings Exploiting Feedforward Control

Marius PAKŠTYS [a], Andrea TONOLI[a], Angelo BONFITTO[a]

[a] Department of Mechanical and Aerospace Engineering – Politecnico di Torino, Duca degli Abruzzi 24, 10129 Turin, Italy (marius.pakstys@polito.it)

Abstract

The present paper focuses on non-linear numerical modeling of active magnetic bearings (AMBs) in a compressor system. The rotor is modeled through a FEM approach and external disturbances are considered as constant and variable loads. Constant loads arise from nominal compressor operation and variable loads are shocks described by a known acceleration profile. Proportional-Integral-Derivative (PID) position controllers are coupled with feedforward (FF) control for the AMBs to mitigate variable load effects on the rotor. FF control is an adaptable static gain dependent on the versus of the imposed shock. Proportional-Integral (PI) current controllers reflect power electronics behaviour. Simulation results indicate that displacements for the most loaded radial AMB are 40% and 44% of the nominal air gap, for negative and positive shocks respectively. Displacements for the axial AMB are 30% and 54% of the nominal air gap for negative and positive shocks respectively. The implemented control scheme proves effective in mitigating the effects of known external disturbances.

Keywords: Active magnetic bearings, Non-linear modeling, PID, Feedforward control, Disturbance rejection

1. Introduction

Active magnetic bearings (AMBs) have become popular for use in rotor systems, due to little maintenance requirements over the span of their operational lifetime. Their implementation is well-suited where ease of access is not guaranteed. The absence of lubricants means that AMBs may be introduced in air conditioning systems. One such case is presented, where a compressor rotor mounted with a single-stage impeller is suspended by two cylindrical AMBs controlling radial displacement in four degrees of freedom (DOFs), and a thrust AMB sustaining axial disturbances in one DOF. Figure 1 indicates the features of interest. This work focuses on an analytical non-linear modeling approach for the electromechanical domain. Previous work has explored non-linear modeling, however quantities were obtained from lookup tables (Tomczuk & Wajnert (2018)). The compressor is mounted on a moving foundation subject to variable external disturbances, which are modeled based on a force estimation method. For radial disturbances, this method makes use of stator acceleration, rotor mass and relative position of AMBs with respect to the centre of mass (COM). In the axial direction, stator acceleration and rotor mass are used to estimate a force. Constant loads are considered as static contributions during modeling.

Stable and safe operation is ensured by the control strategy adopted. A Proportional-Integral-Derivative (PID) position controller with feedforward (FF) control is initialised for each AMB. The present study outlines a FF controller comprised of a static gain dependent on disturbance force direction, allowing for a straightforward application in all actuator axes. A previous study has implemented an adaptable acceleration feedforward, however in a single DOF application (Min Sig Kang & Woo Hyun Yoon (2006)). The behaviour of power electronics is considered by a Proportional-Integral (PI) controller.

The remainder of the work is organised as follows. Section 2.1 briefly discusses rotordynamic modeling. Section 2.2 presents non-linear modeling of the actuators and Section 2.3 indicates the modeling method for constant and variable loads. Section 3 highlights the control strategy adopted and the results of numerical simulations in Simulink®. Section 4 concludes the work.

2. Modeling

2.1 Rotordynamics

Flexural behaviour is modeled with a FEM approach employing DYNROT, a proprietary FEM-based code on MATLAB® developed by Politecnico di Torino. Sensors for radial displacements (x- and y-axes) are located in the immediate vicinity of each radial AMB. An equivalent impeller approximating inertial properties of the original impeller is used, allowing for a simplification in rotor discretisation. The generated state space is characterized by 246 inputs and 16 outputs, considering a nominal rotational speed of 45000 rpm. The first 6 inputs specify x- and y-axis forces at the actuator and impeller nodes. The outputs specify x- and y-axis displacements and velocities of actuator and sensor nodes. Well-known rotordynamic equations of motion serve as a reference (Chen (2015)). A model order reduction is performed in MATLAB® to reduce simulation time, with relevant dynamics conserved for a minimum order of 20. The state space is subsequently implemented into the overall Simulink® model. Dynamics in the z-axis are not present in the state space and are considered separately in the model.

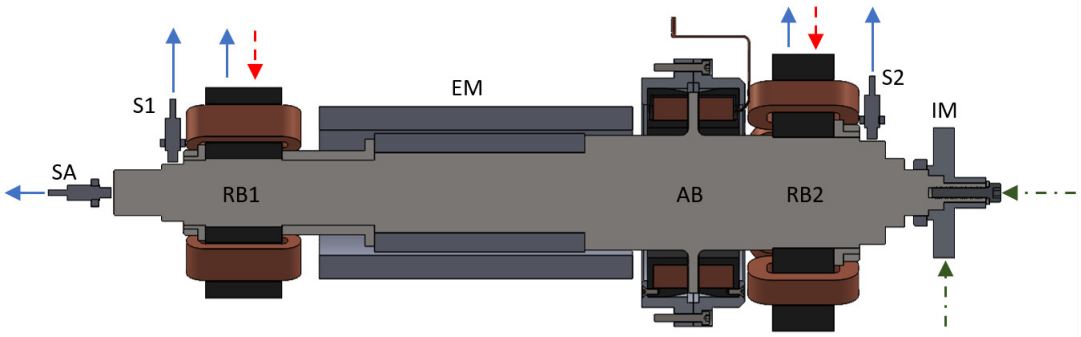

Figure 1: (a) Cross-section of compressor system displaying pertinent features. IM: equivalent impeller. RB1, RB2: radial bearings. AB: thrust bearing. SA: axial sensor. S1: RB1 radial sensor. S2: RB2 radial sensor. EM: electric motor. Outputs in state space model are denoted with solid blue arrows. Dashed red arrows are actuator inputs, and dashed-dot green arrows are impeller inputs.

2.2 Actuators

Actuators are modeled using a set of non-linear analytical expressions. A voltage-based method is used to model the AMBs exploiting Eqs. 1, 2, and 3 (Jeong et al. (2012)), with E denoting the voltage across actuator terminals.

$$E = L(x)\frac{\mathrm{d}i}{\mathrm{d}t} - \frac{L(x)}{(u_0 \pm x)}\dot{x}\cdot i + R\cdot i \tag{1}$$

$$L(x) = \frac{N^2\cdot\mu_0\cdot A}{2(u_0 \pm x)} \tag{2}$$

$$F(i,x) = \frac{N^2\cdot\mu_0\cdot A}{4}\cdot\frac{i^2}{(u_0 \pm x)^2} \tag{3}$$

Note that $L(x)$ is the inductance as a function of displacement x, and i is the coil current that includes the bias current. The terms N and μ_0 are the number of coil turns and vacuum permittivity respectively. The nominal air gap is u_0 and the active magnetic cross section is A. Coil resistance is represented with R, and λ is the magnetic flux. The chosen parameters and physical dimensions for this system yield continuous and peak force limits for the AMBs. Both radial AMBs have a continuous force limit of 400 N, and a peak force limit of 800 N. The axial AMB presents a continuous force limit of 600 N, and a peak force limit of 1100 N.

2.3 Disturbances

External disturbances are introduced as constant and variable loads. Variable loads are shocks following a known acceleration profile. An example is shown in Figure 5b, where the profile is superposed over the displacement. Peak acceleration is 96.1 m/s^2 with a duration of 11.49 ms. Three shocks with a negative versus and three with a positive versus are imposed on each axis of the COM. Stator acceleration in the axial direction is converted to a force using total mass of the rotor, $m = 9$ kg. Analogously, stator acceleration is used to estimate rotor disturbance load for the radial bearings, as presented in Figure 2a. Equation 4 indicates forces on the rotor, with $\ddot{q}_r$ and $\ddot{q}_s$ being general rotor and stator radial accelerations respectively. Net AMB force on the rotor is F_{AMB} and rotor weight is F_W. Relative position of AMBs with respect to rotor COM is used to split the inertial load stemming from stator acceleration, shown in Figure 2b. Forces on bearings RB1 and RB2 are given by Eqs. 6 and 7 respectively. The distances of bearings RB1 and RB2 relative to the COM are $a = 180$ mm and $b = 114$ mm respectively. This approach is possible if the external accelerations are known *a priori*.

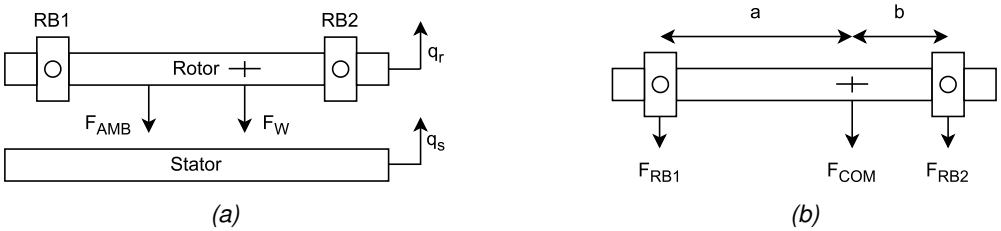

Figure 2: (a) Simplified free body diagram of rotor and stator. (b) Free body diagram of rotor indicating relative positions of radial AMBs with respect to COM.

$$m(\ddot{q}_r - \ddot{q}_s) = F_{AMB} + F_W \tag{4}$$

$$F_{COM} = m \cdot \ddot{q}_s \tag{5}$$

$$F_{RB1} = m \cdot \ddot{q}_s \frac{b}{a+b} \tag{6}$$

$$F_{RB2} = m \cdot \ddot{q}_s \frac{a}{a+b} \tag{7}$$

The static unbalance effect is introduced using a sinusoidal force term. It is assumed to act on the COM, hence the aforementioned procedure adopted for variable disturbances is used to assign load contributions to radial AMBs. The unbalance grade is $G = 2.5$ mm/s for compressors, as per ISO 1940-1 (ISO-1940-1:2003 (2003)). The corresponding maximum permissible eccentricity is $\varepsilon = 0.53$ μm.

Constant loads are implemented directly as known forces from compressor operation. Forces of 100 N in the x- and y-axes of the impeller node are considered as inputs in the state space model. A force of 300 N is imposed in the z-axis. Rotor weight contributes to the y-axis of each radial AMB and is split in the same manner as variable loads.

3. Control Strategy and Simulation Results

The strategy implemented for position control is a combination of feedback and feedforward logic. Feedback control is characterised by a PID controller (Anantachaisilp et al. (2012)), while FF control is an adaptable static gain that is exploited for shocks. The FF gain is sensitive to the versus of imposed acceleration, as constant net forces cause varying instantaneous loads in either positive or negative directions. The FF scheme is evidenced in Figure 3. Each AMB features its own PID and FF controller, describing a decentralised control architecture. A PI current controller is included for each AMB, with the output bounded by the DC bus voltage, $V_{DC} = \pm 50$ V. Figure 4 summarises the control layout implemented for the AMBs. Previous non-linear modeling is used as a reference (Tomczuk & Wajnert (2018)). Current and position controllers are modeled as filters, dependent on

the Laplace variable s. The current controller C_c in Eq. 8 contains the proportional gain $K_{p,c}$, and the integral time constant $T_{i,c}$. The position controller in Eq. 9 contains the proportional gain $K_{p,p}$, the integral time constant $T_{i,p}$, and the derivative time constant T_d. A closing pole factor N_d is additionally included.

The parameters for position control are chosen on the basis of the rigid-body mode frequency in closed loop. The closed loop transfer function considers node displacement as the output, and external force on the actuator as the input. The parameters yield rigid body modes at 100 Hz with a gain of -125 dB for the radial AMBs. For the axial AMB, a frequency of 60 Hz and a gain of -120 dB is noted. The frequencies indicate a stiff behaviour of the system ensuring that the position controllers are operationally suitable for the provisioned external excitations. Current controller parameters are chosen such that they exhibit a zero at 5.3 Hz for the axial AMB, and 6.4 Hz for both radial AMBs.

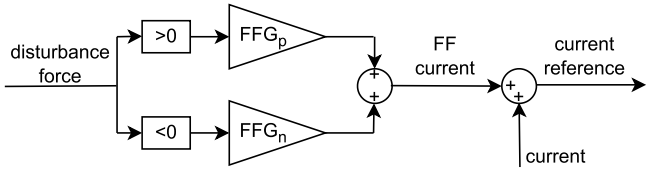

Figure 3: FF control logic for gain adaptation. FFG_p: gain for positive shocks. FFG_n: gain for negative shocks.

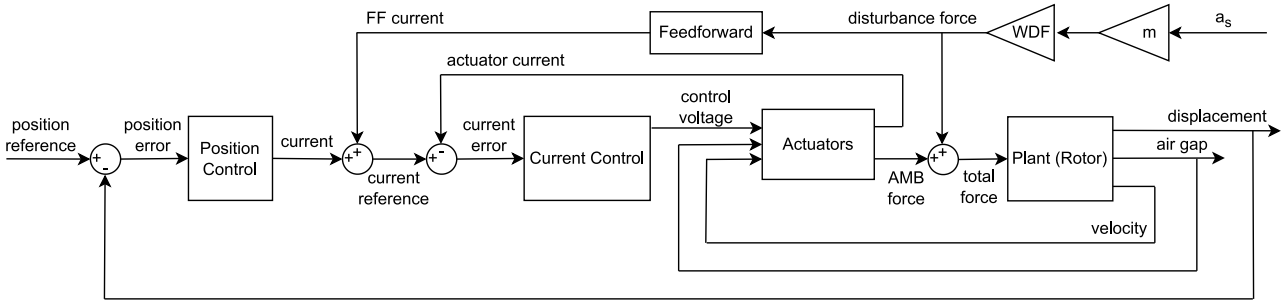

Figure 4: Non-linear control scheme for AMBs. a_s: stator acceleration. WDF: weight distribution factor calculated as per the relative position of radial AMB with respect to COM.

$$C_c = K_{p,c}\left(1 + \frac{1}{T_{i,c}s}\right) \tag{8}$$

$$C_p = K_{p,p}\left(1 + \frac{1}{T_{i,p}s} + \frac{T_d s}{1 + \frac{T_d}{N_d}s}\right) \tag{9}$$

The Simulink® model generates numerical responses due to combined constant and variable loads. Figure 5a highlights the net force experienced by RB1 in the y-axis. The first three peaks are positive net forces that counteract the negative shocks imposed. A constant force offset accounts for rotor weight and radial compressor load at the impeller node. Figure 5b displays the y-axis node displacement of RB1 due to the first negative shock, with a peak displacement of -0.15 mm, corresponding to 30% of the nominal air gap. For an imposed positive shock, node displacement covers 46% of the air gap.

Net force in the y-axis of RB2 is shown in Figure 6a. The continuous force limit is surpassed with a maximum duration of 12 ms. The force limit reflects the permissible current in the coils, such that actuator damage due to Joule losses is avoided. The duration is noted to be insufficient to induce overheating. The y-axis node response of RB2 is shown in Figure 6b with a peak displacement of -0.20 mm, referring to 40% of the nominal air gap. Displacement in the positive direction corresponds to 44% of the air gap.

Figure 7a indicates net forces exerted by the axial AMB. Shocks require a force request that surpasses the continuous force limit, however the duration of 11.6 ms is insufficient to induce coil overheating during operation.

The performance of AB is adequate, confirmed by node displacement due to the first negative shock in Figure 7b. A peak displacement of -0.15 mm is noted, corresponding to 30% of the nominal air gap. With a positive shock, node displacement covers 54% of the air gap. In all cases the PID and FF controller combination is observed to ensure a restoration of steady state displacement. All bearings suitably sustain constant loads, remaining below the continuous force limit.

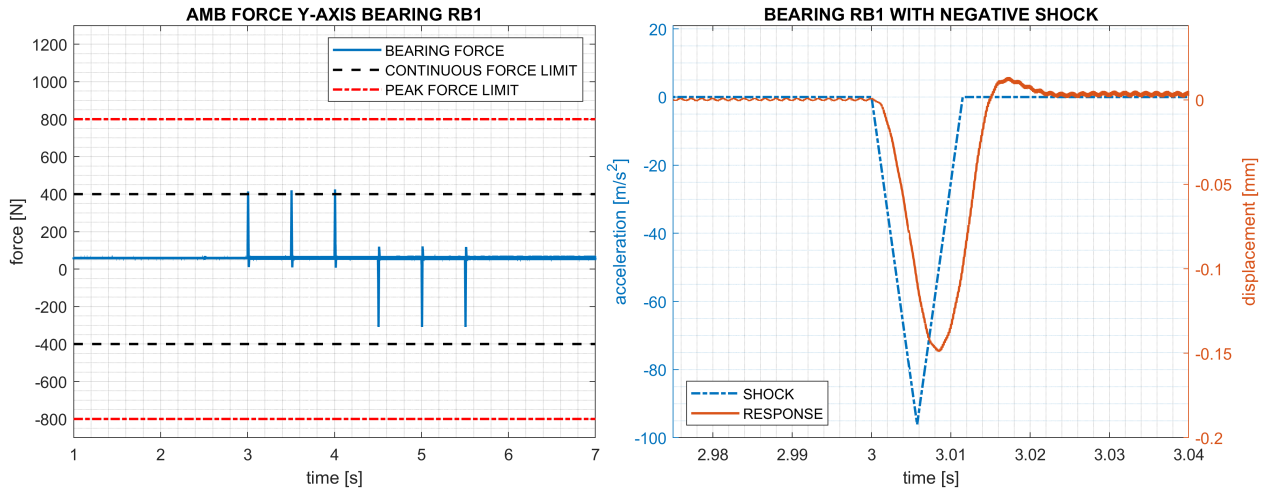

(a) *(b)*

Figure 5: (a) Forces experienced by RB1 in y-axis due to shocks, constant radial compressor loads, and effect of static unbalance.

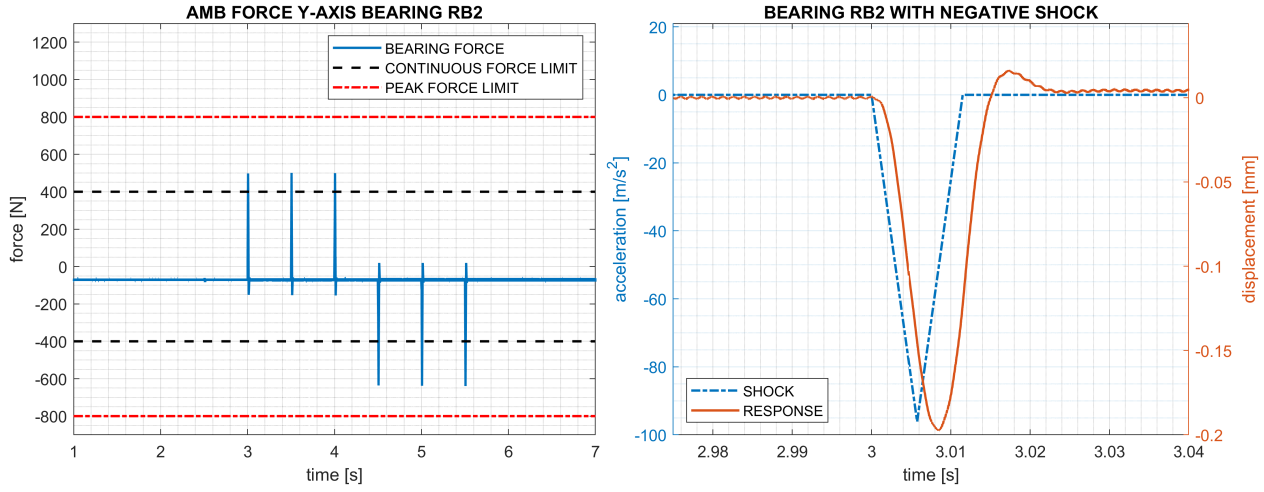

(a) *(b)*

Figure 6: (a) Forces experienced by RB2 in y-axis due to shocks, constant radial compressor loads, and effect of static unbalance.

4. Final remarks

The modeling approach for a compressor rotor suspended by AMBs has been outlined, with non-linear analytical modeling for the electromechanical domain, and a FEM modeling approach for rotordynamic behaviour. Constant and variable loads are modeled, including rotor weight and static unbalance. An adaptive FF control

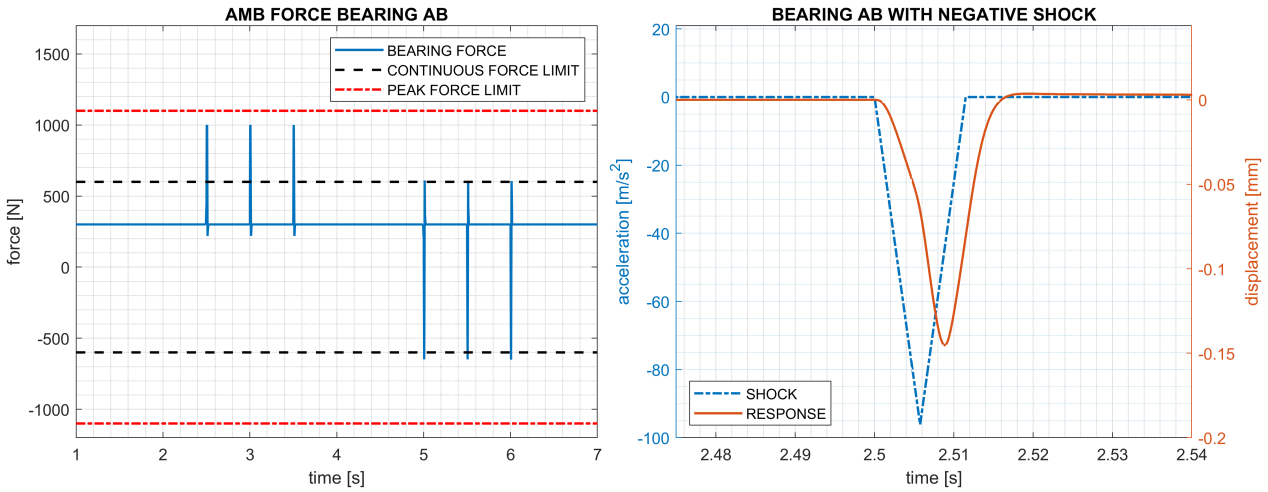

(a) *(b)*

Figure 7: (a) Forces experienced by bearing AB in z-axis due to shocks and constant axial compressor load.

complements the PID position controller for each AMB. Numerical results indicate a stable response to imposed shocks, confirming the operational viability of the system. Knowledge of the shock profile is required, making this control approach suitable for well-studied applications. Deviations from the expected variable loading may not be adequately sustained by the controller, presenting a limitation to general applications. Further work involves an analysis of the robustness of such control. The choice of PID gains may be informed by a deeper exploration of system stability, observing the closed-loop poles and applying the Nyquist stability criterion. A more general force estimation method may also be included, to account for environments with unknown inputs. An experimental validation to assess the modeling method is also required.

References

Anantachaisilp, P., Lin, Z. & Allaire, P. (2012), Pid tuning methods for active magnetic bearing systems, *in* '13th International Symposium on Magnetic Bearings', Arlington, Virginia, USA, pp. 1–14.

Chen, W. J. (2015), *Practical Rotordynamics and Fluid Film Bearings*, 1 edn, Trafford Publishing.

ISO-1940-1:2003 (2003), Mechanical vibration – balance quality requirements for rotors in a constant (rigid) state, Standard ISO 1940-1:2003, International Organization for Standardization, Geneva, CH.

Jeong, H. H., Yun, S. N. & Yang, J. H. (2012), Control of magnetic bearing system, *in* R. Sehgal, ed., 'Performance Evaluation of Bearings', IntechOpen, Rijeka, chapter 8.
URL: *https://doi.org/10.5772/51185*

Min Sig Kang & Woo Hyun Yoon (2006), 'Acceleration feedforward control in active magnetic bearing system subject to base motion by filtered-X LMS algorithm', *IEEE Transactions on Control Systems Technology* **14**(1), 134–140.
URL: *http://ieeexplore.ieee.org/document/1564103/*

Tomczuk, B. & Wajnert, D. (2018), 'Field–circuit model of the radial active magnetic bearing system', *Electrical Engineering* **100**(4), 2319–2328.
URL: *http://link.springer.com/10.1007/s00202-018-0707-7*